Applied Catalysis B: Environmental 184 (2016) 104–118

Contents lists available at ScienceDirect

Applied Catalysis B: Environmental

journal homepage: www.elsevier.com/locate/apcatb

Catalytic applications of alkali-functionalized carbon nanospheres and their supported Pd nanoparticles

Yibo Yan[a], Yihu Dai[a], Shuchao Wang[a], Xinli Jia[a], Hao Yu[b,**], Yanhui Yang[a,*]

[a] School of Chemical and Biomedical Engineering, Nanyang Technological University, Singapore 637459, Singapore
[b] The School of Chemistry and Chemical Engineering, South China University of Technology, Guangzhou 510640, China

ARTICLE INFO

Article history:
Received 31 July 2015
Received in revised form
16 November 2015
Accepted 18 November 2015
Available online 28 November 2015

Keywords:
Carbon nanospheres
Surface functionalization
Benzyl alcohol oxidation
Glycerol oxidation
Aldol condensation

ABSTRACT

Carbon nanospheres (CNSs) prepared by hydrothermal approach and post-functionalization with alkali solutions were employed as solid base catalysts in aldol condensation. The negative charge and alkalinity of CNS surfaces were controlled by the concentration of alkali solutions, leading to the high selectivity superior to aqueous NaOH as the traditional catalyst. Furthermore, CNSs with varying surface alkalinity can be adopted as proper supports for highly dispersed Pd nanoparticles with well-controlled size distribution. The optimized alkaline CNS-supported Pd catalysts demonstrated enhanced reactivities in the solvent-free selective oxidation of benzyl alcohol and the aerobic oxidation of glycerol. In-depth characterizations of their structural and electronic properties by transmission electron microscope (TEM), field emission scanning electron microscope (FESEM), Fourier transform infrared spectroscope (FTIR) and X-ray photoelectron spectroscopy (XPS) were performed to elucidate the nature of the active sites and the mechanism. The effect of electron density, size of Pd nanoparticles as well as the surface alkalinity of supports on the catalytic performance has been unveiled.

1. Introduction

Since the first discovery of carbon nanotubes [1], plenty of efforts have been made to create diversified morphologies of carbon materials, such as hollow coin-like carbons [2], carbon nano-fibers [3], graphene [4], graphene-nanotube fibers [5] and so on. Among these carbon materials with different structures, carbon nanospheres (CNSs) have attracted tremendous attention because of their important roles in catalyst supports [6–8], adsorbents [9–11], photonic band-gap crystals [12], electrode materials for lithium ion batteries [13–15], and template materials for fabricating hollow/core-shell metallic or nonmetallic spheres [16–18]. Various methods have been developed to synthesize carbon spheres including chemical vapor deposition (CVD) [19], pressure carbonization [20], mixed-valence oxide-catalytic carbonization [21], and reduction of carbides with metal catalysis [22].

A "green" synthetic approach free of toxic reagents and organic solvents has been established to transform the readily prepared precursors including glucose [23–25], starch [26] and cyclodextrins solutions [27] to generate carbon spheres by simply using hydrothermal vessels at the temperature ranged from 160 to 180 °C. The diameters of CNSs were influenced by temperature, reaction duration and the concentration of precursor solutions. At constant temperature, diameter and size distribution increased with the increase of reaction time and peanut-like or other irregular shapes occurred at long reaction time duration. High concentration of precursor solution usually led to large diameters and broader size distributions [24,28]. Concerning temperature issues, Li et al. reported that the diameter decreased when the temperature increased from 180 to 190 °C while broken or irregular shapes of CNSs appeared at 210 °C using 0.3 M glucose solution [28].

The surface of the as-synthesized CNSs comprised abundant hydrophilic surface functional groups including C—OH, C=O and —COOH groups which can enable the promising application of CNSs for water-treatment adsorbent [9,29,30]. Other applications involved the support materials for metal or metal oxides ascribed to the strong adsorbent capacitance of metallic ions [24,25,31] as well as the template materials to synthesize hollow/core-shell metal spheres or metal oxide spheres [32,33]. The surface properties and composition of carbon spheres can be well-modified through chemical treatment with a wide variety of reagents such as oxidants, acids, bases, polymers and so forth [9]. Owing to the precursors, the surfaces of CNSs were decorated with plentiful C—OH and C=O groups, the density of which can be altered by

* Corresponding author. Fax: +65 67947553.
** Corresponding author. Fax: +86 20 8711 4916.
E-mail addresses: yuhao@scut.edu.cn (H. Yu), yhyang@ntu.edu.sg, yanhui.yang@live.com (Y. Yang).

http://dx.doi.org/10.1016/j.apcatb.2015.11.024
0926-3373/

similar chemical treatment in acids or bases solutions in order to further improve the adsorption capacitance. For the functionalization with carboxyl groups, adding acrylic acid monomer during the hydrothermal synthesis of CNSs has been reported to prepare the carboxyl-groups-functionalized carbon spheres [29]. Another approach to synthesize CNSs surface functionalized with carboxyl groups was through the post-synthesis acid treatment, leading to carbon spheres covered with —SO_3H and —COOH functional groups, which has been subsequently utilized as the solid-acid catalysts for typical acid-catalyzed reactions such as the hydrolysis of polysaccharides [34]. Up to now, there was no literature reporting the treatment of CNSs in order to prepare the solid base catalysts for base-catalyzed reactions (i.e., Michael addition, alkylation, isomerization, Knoevenagel, adol and Claisen–Schmidt condensations, etc.) which were commonly catalyzed by either sodium hydroxide or potassium hydroxide [35].

Besides, regarding the strong metal adsorption capacitance of CNSs [9] and its flexibility of surface modification, functionalized CNSs may serve as excellent catalytic support for specific reactions such as selective oxidation of benzyl alcohol [36,37]. In addition, selective oxidation of glycerol has attracted tremendous attention because the expanding regenerative biodiesel production gives rise to a large amount of glycerol as an inexpensive by-product and the glycerol oxidation is a procedure under mild conditions to efficiently transform glycerol into valuable chemicals such as glyceric acid, hydroxypyruvic acid, tartronic acid and dihydroxyacetone [38–41]. Herein, the investigation concerning the surface-functionalized CNSs serving as the solid base catalyst for aldol condensation and also the catalytic support of highly dispersed Pd nanoparticles for selective oxidation of benzyl alcohol and aerobic oxidation of glycerol is going to be unraveled in this study (Scheme 1). Their structures and properties are characterized via field emission scanning electron microscope (FESEM), transmission electron microscope (TEM), Brunauer–Emmett–Teller (BET), X-ray Diffraction (XRD), RAMAN, Fourier Transform infrared spectroscopy (FTIR), X-ray photoelectron spectroscopy (XPS), inductively coupled plasma (ICP) and zeta potential measurement.

2. Experimental

2.1. Synthesis of CNSs

The preparation method of CNSs referred to the hydrothermal approach reported in the literatures [9,24]. Alpha-D(+)-glucose (3.6 g, Sigma, 99.5%, anhydrous) was dissolved in ultrapure water to afford 40 mL of 0.5 M aqueous solution via ultrasonication for 30 min prior to the hydrothermal synthesis in a Teflon-lined autoclave at 160 °C for 12 h. The as-synthesized CNSs were rinsed with ultrapure water and ethanol for several times followed by drying at 60 °C overnight.

2.2. Functionalization of CNSs in sodium hydroxide aqueous solutions

The pristine CNSs were then surface-functionalized via immerging into sodium hydroxide aqueous solutions. 0.24 g of dry CNSs powder was dispersed in 200 mL of sodium hydroxide solution of specific concentration. The suspension was vigorously stirred at 600 rpm at room temperature for 1 h, and then was collected via filtration and rinsed with deionized water until the pH of the filtrate was neutral. The functionalized CNSs were dried at 60 °C for 12 h. functionalized CNSs were denoted as CNS-*x*OH where *x* referred as the molar concentration of sodium hydroxide concentration. The CNSs sample without treatment was denoted as CNS.

2.3. Functionalization of CNSs with Pd nanoparticles

Palladium nanoparticles supported on functionalized CNSs were synthesized by the well-established adsorption–reduction method [36]. $PdCl_2$ aqueous solution (767.1 μL of 0.05 M) and 0.2 g of functionalized CNSs were suspended in 20 mL of deionized water followed by stirring at room temperature for 2 h. The palladium ions were reduced by adding excess amounts of 1 M $NaBH_4$ under the protection of nitrogen and stirred overnight. Then the suspension was centrifuged, rinsed with deionized water and dried in a vacuum oven.

2.4. Sample characterization

Powder X-ray diffraction (XRD) patterns were obtained on a Bruker AXS D8 diffractometer using a filtered Cu Kα radiation (λ = 0.15406 nm) source at 40 mA and 40 kV under ambient condition. The XRD data were collected from 10 to 80° (2θ) with a resolution or step of 0.02° (2θ). The morphology and texture were observed with field emission scanning electron microscope JEOL 6700F (FESEM). Transmission electron microscope (TEM) JEOL JEM-2100F was operated at 200 kV, with sample suspension in ethanol dropped and dried onto Cu grid. The surface area and pore volume were obtained using the adsorption isotherms of nitrogen at −196 °C on a Quantachrome Aurosorb-6B apparatus. The X-ray photoelectron spectroscopy (XPS) measurement was obtained on a VG Escalab 250 spectrometer together with the Al Kα 1846.6 eV anode. C 1s peak at 284.6 eV was the reference for binding energy calibration. Surface functional groups on the samples were investigated with PerkinElmer Fourier transmission infrared spectroscopy (FTIR, Spectrum 1), with samples homogeneously pressed into KBr pellets. Raman spectra were monitored on a Renishaw Raman spectrometer using an Ar excitation laser light with the wavelength of 514.5 nm, and the detection depth is around 150 nm. Zeta potential was measured with 12.5 mg of samples dispersed in 25 mL of pH buffer solution (pH = 7.00 ± 0.02) using a zeta potential analyzer BIC PALS. The metal contents were measured by the inductively coupled plasma (ICP). Nitric acid was utilized to dissolve the samples. The pH value of functionalized CNSs were measured following the method reported elsewhere [36]. The sample (0.2 mg) was suspended in 10 mL of boiling distilled water, boiled for 5 min, followed by cooling to room temperature and stirring overnight to attain balance. After filtration, the pH value of the filtrate solution was measured by a pH meter. The elemental analysis for the content of each non-metallic element has been performed on a vario EL *III* Elementar.

2.5. Catalytic reactions

Aldol condensation was conducted according to the following procedures. Benzaldehyde (1 mL) was added to 1 mL of acetaldehyde, 0.1 g of catalyst, 10 mL of deionized water and 5 mL of ethanol. The reaction was carried out in a Teflon-lined hydrothermal reactor for 5 h under the protection of nitrogen gas flow. After the reaction, the suspension was centrifuged and the organic phase was analyzed by the Agilent gas chromatography installed with a HP-5 column. The control experiment was also performed using 20 mL of NaOH aqueous solutions of certain concentrations (0.01, 0.05, 0.07, 0.1, 0.2, 0.5 and 0.7 M, respectively denoted as NaOH-0.01 M, NaOH-0.05 M, NaOH-0.07 M, NaOH-0.1 M, NaOH-0.2 M, NaOH-0.5 M and NaOH-0.7 M) instead of the mixture of CNSs and deionized water.

The solvent-free oxidation of benzyl alcohol with oxygen flow was conducted in a bath-type reactor under ambient pressure. Benzyl alcohol (0.05 mol, 5.174 mL) was loaded into a three-necked flask pre-charged with 0.01 g of catalyst. The flask was soaked in a silicone oil bath at 120 °C with the oxygen bubbled at the

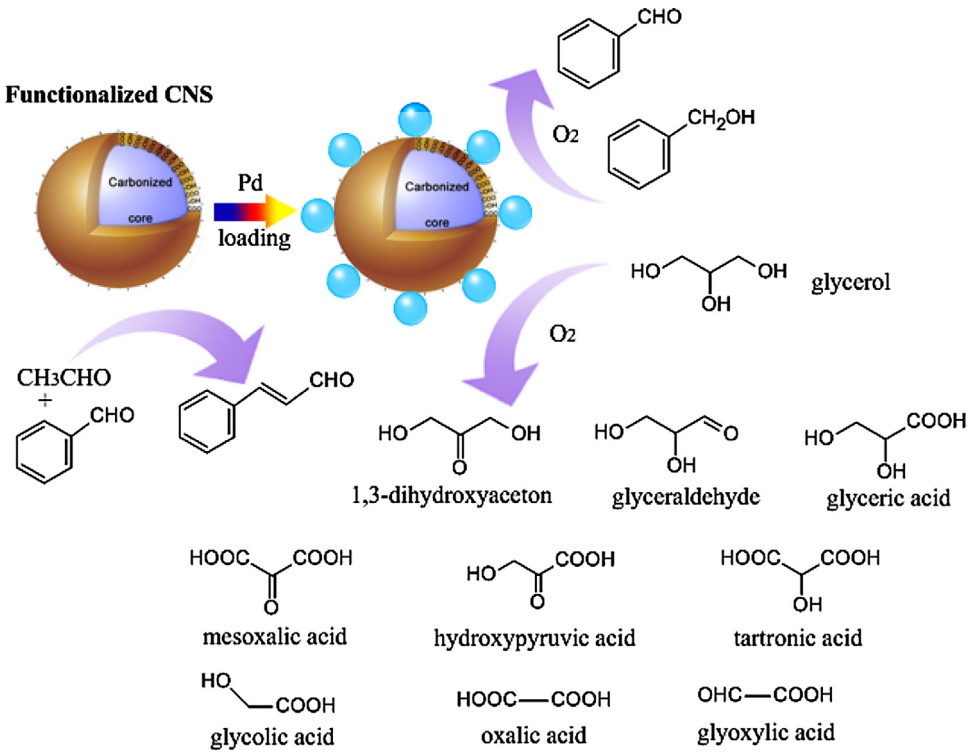

Scheme 1. Schematic illustration of catalyst preparation and catalytic application of surface-functionalized CNS based catalysts.

rate of 20 mL/min to initiate the reaction. The reaction continued for 8 h under magnetic stirring at 1200 rpm. The suspension was centrifuged with the liquid phase analyzed by the Agilent gas chromatography (GC 6890) installed with a HP-5 capillary column. The dodecane was employed as a standard to measure the percentage of each products and residual reactant so as to evaluate the conversion of reactant and the selectivity toward main product [42]. The calculation of conversion, selectivity and quasi-turnover frequency (qTOF) were described elsewhere [43].

Selective oxidation of glycerol was carried out in a three-necked flask with a bubbled gas supplied system, condenser, magnetic stirring and thermocouple. The glycerol aqueous solution (20 mL of 10 wt.%) and 50 mg of catalyst were added to the flask. Oxygen was purged into the liquid at 150 mL/min by mass flow controller. After the reaction, catalyst was filtered off and liquid phase was charged into a 50 mL flask and analyzed by a high performance liquid chromatography (HPLC, Agilent 1260 Infinity) armed with variable wavelength detector (VWD, G1314B, 1260 VWD VL), refractive index detector (RID, G1362A 1260), thermostatted column compartment (TCC, G1316A), G1322A standard degasser and Alltech OA-1000 Organic Acid HPLC Column was used with the diluted 4 mmol/L sulfuric acid as the eluent. Prior to the HPLC analysis, each of the glycerol (>99.0%), 1,3-dihydroxyacetone dimer (DHA, 98%), glyceric acid (GLYA, 40 wt.% aqueous solution), glycolic acid (GLYCA, 98%), glyceraldehyde (GLYHD, 95%), hydroxypyruvic acid (HPYA, 95%), oxalic acid (OXA, 98%), tartronic acid (TARAC, 95%), mesoxalic acid (MOXA, 98%) and glyoxylic acid (GLYOA, 98%) were run individually for calibration of the standard retention time of each possible product.

The carbon balances have been calculated according to the equation with tetradecane (n-$C_{14}H_{30}$) as the inert standard:

$$\text{carbon balance} = \frac{\left[(\text{GC peak area of product} + \text{reactant residual})/(\text{corresponding tetradecane peak area after reaction})\right]}{\left[(\text{GC peak area of reactant before reaction})/(\text{GC peak area of reactant before reaction})\right]} \times 100.$$

The definition of conversion, selectivity and turnover frequency (TOF) are as follows:

$$\text{Conversion}\,(\%) = \frac{(\text{Moles of reactant converted})}{(\text{Moles of reactant in feed})}$$

$$\text{Selectivity}\,(\%) = \frac{(\text{Moles of product formed})}{(\text{Moles of reactant converted})}$$

$$\text{TOF}\left(\text{h}^{-1}\right) = \frac{(\text{Moles of product converted})}{(\text{Moles of Pd} \times \text{reaction time}\,(\text{h}))}$$

3. Results and discussion

3.1. Characterizations of the as-prepared functionalized CNSs

Fig. 1A shows the TEM and FESEM images of the as-synthesized CNSs sample. The diameters of CNSs are ranged from 50 to 300 nm, similar to the result reported by Song et al. [9]. The hydrothermally synthesized CNSs are nonporous as evidenced by the low specific surface area (35.5 m^2/g) and pore volume (0.03 mL/g) [9,23–25]. No noticeable changes in the surface area, pore volume and morphology occur upon the surface functionalization by NaOH solutions at room temperature, which is different from the high-temperature treatment of CNSs using solid alkali [44]. Raman spectroscopy is employed to characterize the functionalized CNSs and the results are shown in Fig. 2. The graphitic G-band at 1580 cm^{-1}, is ascribed to the graphite-oriented Raman-active E_{2g} mode [45,46]. The disordered carbon-oriented D-band at 1370 cm^{-1} is due to the structural defect, finite size effect and lattice distortion of CNSs [47], which is weak for the pristine CNSs and even weaker for

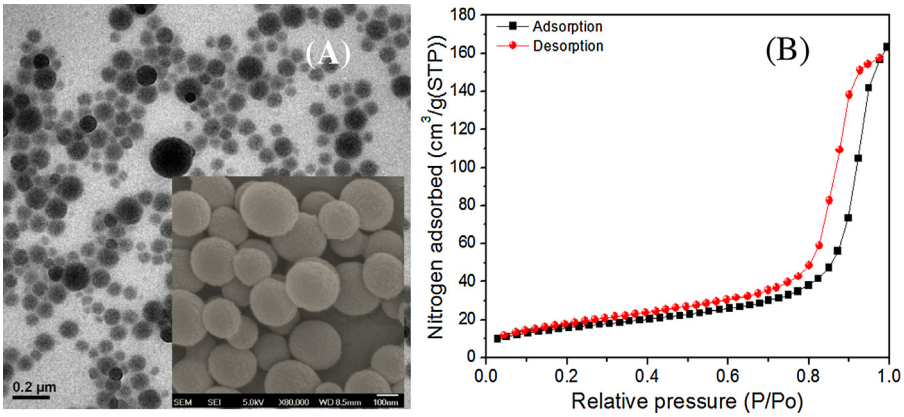

Fig. 1. (A) TEM and FESEM observations of the as-synthesized CNSs and (B) nitrogen adsorption–desorption isotherm of CNSs.

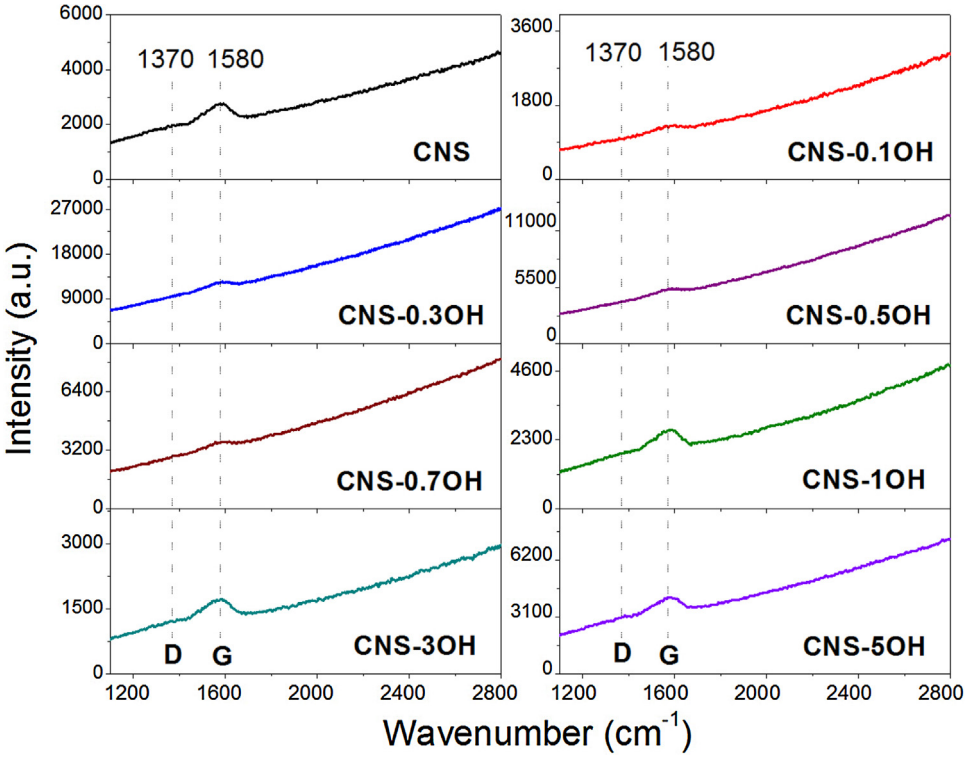

Fig. 2. Raman spectra of CNS, CNS-0.1OH, CNS-0.3OH, CNS-0.5OH, CNS-0.7OH, CNS-1OH, CNS-3OH and CNS-5OH catalysts.

the NaOH-functionalized CNSs. Sun et al. reported that the CNSs were hydrothermally formed in two steps: glucose polymerization and aromatization/carbonization, resulting in the carbonized core and hydrophilic sugar-polymerized surface [24]. Raman results in this study imply that the highly ordered carbonized core is the major content of the CNSs bulk volume and NaOH functionalization consumes the surface non-carbonized or amorphous carbon species.

The FTIR spectra of NaOH-functionalized CNSs are displayed in Fig. 3. The strong absorption band from 3100 to 3400 cm^{-1} is attributed to the O—H stretching vibration which may overlap with the O—H stretching vibration of water molecules, implying the strong hydrophilicity of CNSs surfaces. The band centered at 1700 cm^{-1} is the stretching vibration of C=O in lactone groups [48], aldehyde groups [49] or carboxyl groups [29,50–53]. The band at 1600 cm^{-1} is the fingerprint of C=C stretching vibrations, while the minor peaks at around 2923 cm^{-1} imply the presence of aliphatic —CH. The bands at 1023 and 1367 cm^{-1} is for the C—OH stretching vibration and the symmetric stretching vibration of the deprotonated carboxylate group —COO^-, respectively [9]. Noticeable increase in the peak intensity of the stretching vibrational band of deprotonated carboxylate group —COO^- at 1367 cm^{-1} occurs as the functionalization alkali concentration increases. As shown in Scheme 2 the NaOH solution can catalyze the hydrolysis of lactone and deprotonate the carboxyl groups, which is constantly employed to explain the decrease in the 1700 cm^{-1} band strength of the lactone C=O stretching vibration and the increase in the intensity of the 1367 cm^{-1} peak derived from the deprotonated carboxylate group —COO^- as the base concentration increases [54–56]. In addition, Cannizzaro reaction, the base-induced disproportionation of an aldehyde without alpha hydrogen, such as the aldehyde groups on aromatic rings formed by the carbonization step, occurs simultaneously to generate hydroxyl and deprotonated carboxylate groups in alkali solutions [57]. Generally, the higher the alkali concentration, the more deprotonated —COO^- groups are generated.

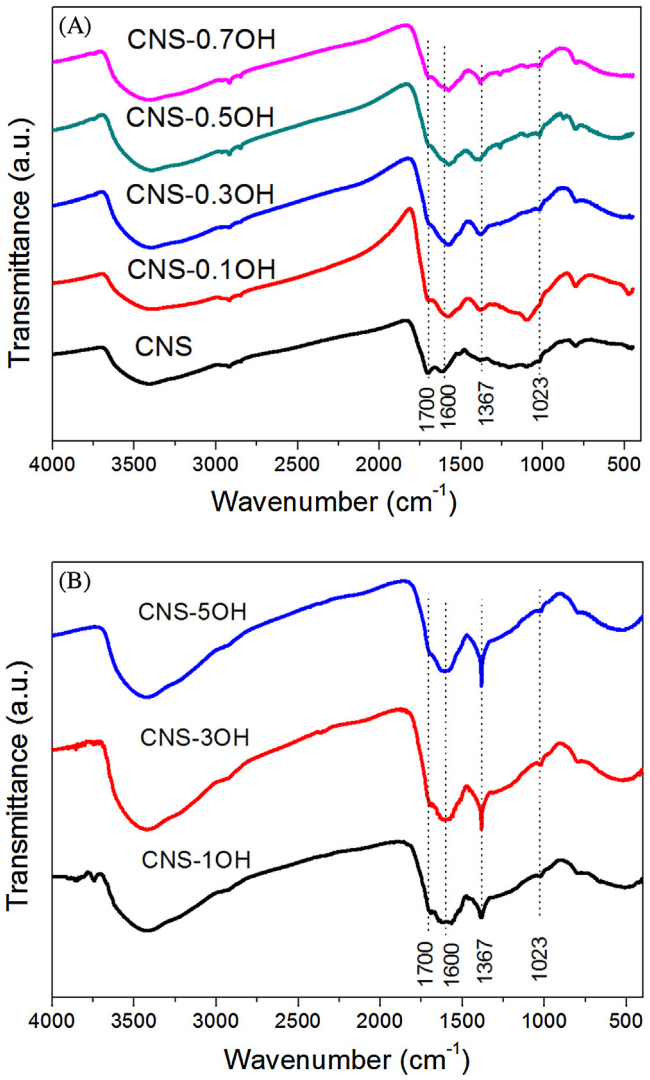

Fig. 3. FTIR spectra of CNS, CNS-0.1OH, CNS-0.3OH, CNS-0.5OH CNS-0.7OH, CNS-1OH, CNS-3OH and CNS-5OH catalysts.

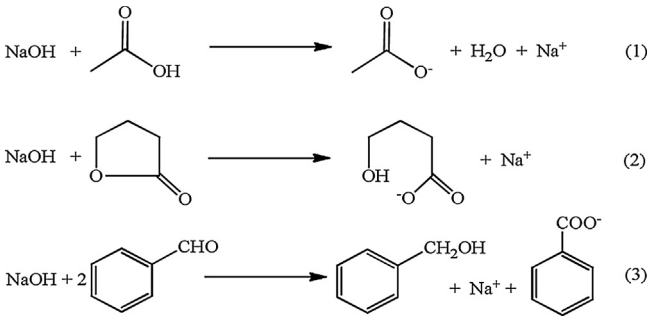

Scheme 2. The NaOH induced reactions on CNS surface during alkali treatment.

The XPS core level spectra of O 1s has been monitored and deconvoluted as shown in Fig. 4. The band assignment is as follow: C═O band within 531.5–532.5 eV, C—O band within 533–536 eV and the lattice oxygen within 529.8–530.1 eV [43]. The O 1s XPS spectra reveal the significant escalation in the value of C═O/C—O fraction: 0.7, 2.4, 4.2, 6.6 and 8.4 for CNS, CNS-0.1OH, CNS-0.3OH, CNS-0.5OH and CNS-0.7OH, respectively. The two O atoms are the same in the deprotonated —COO^- group due to the p–π conjugation structure, one —COO^- group doubles the strength of C═O peak and the emergence of —COO^- shifts the C═O band toward higher binding energy. The significant increase in the C═O/C—O fraction with the increase of alkali concentration further substantiates the occurrence of the alkali-catalyzed deprotonation of carboxyl groups and hydrolysis of lactone to form hydroxyl as well as the deprotonated —COO^- groups.

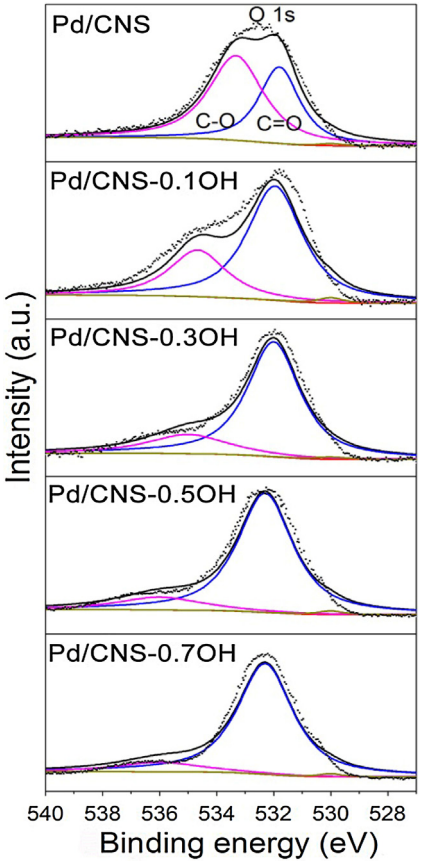

Fig. 4. XPS spectra of O 1s in Pd/CNS, Pd/CNS-0.1OH, Pd/CNS-0.3OH, Pd/CNS-0.5OH and Pd/CNS-0.7OH catalysts.

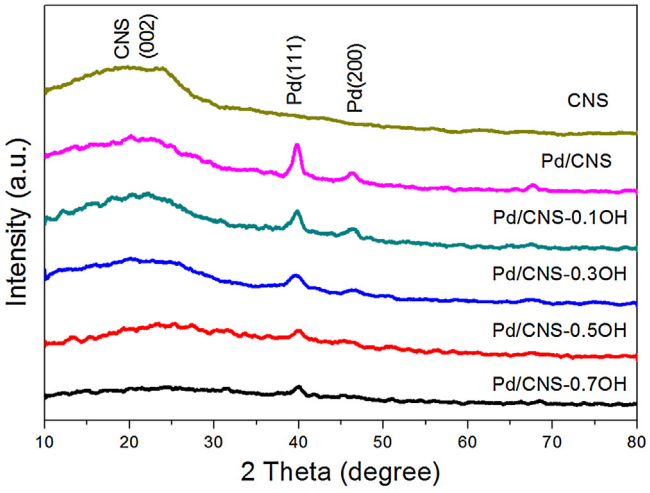

Fig. 5. XRD patterns of CNS, Pd/CNS, Pd/CNS-0.1OH, Pd/CNS-0.3OH, Pd/CNS-0.5OH and Pd/CNS-0.7OH catalysts.

As shown in Tables 1 and 2, the zeta potentials of CNS, CNS-0.1OH, CNS-0.3OH, CNS-0.5OH, CNS-0.7OH, CNS-1OH, CNS-3OH and CNS-5OH dispersed in deionized water have been measured with the results being −26.8 mV, −37.6 mV, −41.8 mV, −43.9 mV,

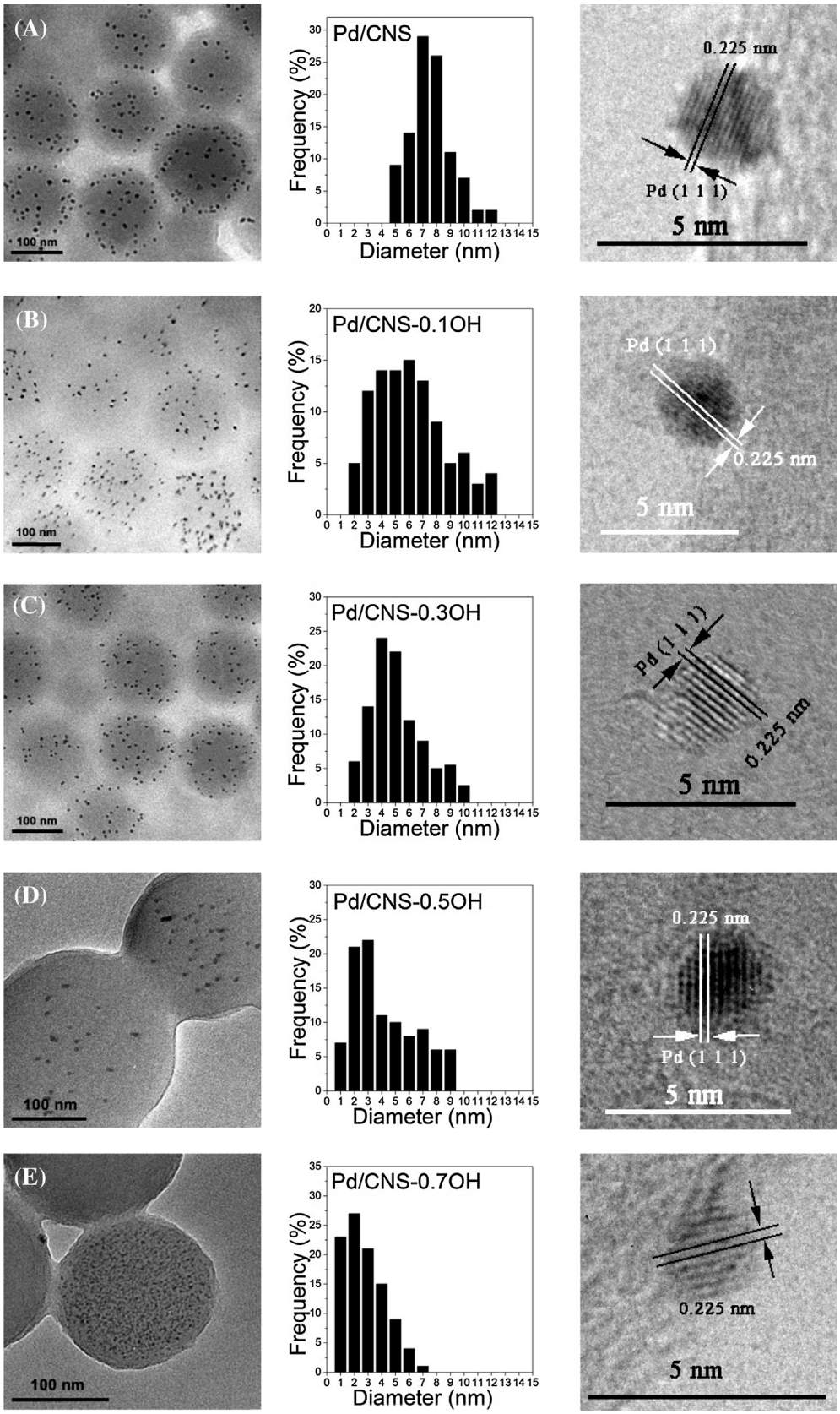

Fig. 6. TEM, HRTEM images and Pd particle size distribution histograms of (A) Pd/CNS; (B) Pd/CNS-0.1OH; (C) Pd/CNS-0.3OH; (D) Pd/CNS-0.5OH and (E) Pd/CNS-0.7OH catalysts; for A to D observations, each sample took 350 NPs into account for size measurement, while E observation used 400 NPs for size measurement considering the small-size-oriented deviation.

Table 1
Zeta potential, pH and catalytic results of aldol condensation over CNS-1OH, CNS-3OH and CNS-5OH.[a]

Entry	Catalyst	ζ Potential (mV) before reaction	ζ Potential (mV) after reaction	pH	C/O weight ratio[c]	Conversion (%)	Yield (%)			Carbon balance of[d]
							cis- + trans-	cis- + trans-	cis- + trans-	
1	[a]CNS-1OH	−47.9	−46.5	9.8	1.81	23.7	23.7	0	0	97.6%
2	CNS-3OH	−50.9	−49.1	10.1	1.77	32.0	32.0	0	0	97.7%
3	CNS-5OH	−52.3	−51.4	10.7	1.70	28.1	28.1	0	0	97.4%
4	[b]NaOH-0.01M			12.0		41.9	41.2	0.7	0	96.6%
5	NaOH-0.05M			12.7		68.3	66.7	1.6	0	95.8%
6	NaOH-0.07M			12.8		69.5	67.3	2.1	0.1	95.3%
7	NaOH-0.1M			13.0		74.6	71.1	3.3	0.2	93.1%
8	NaOH-0.2M			13.3		79.5	69.0	9.4	1.1	92.9%
9	NaOH-0.5M			13.7		87.2	68.7	16.5	2.0	91.5%
10	NaOH-0.7M			13.8		79.8	65.0	11.8	3.0	90.1%

[a] Reaction conditions: CNS, 0.1 g; H_2O, 10 mL; ethanol, 5 mL; benzaldehyde, 1 mL; acetaldehyde, 1 mL; inert nitrogen atmosphere; stirring rate, 1200 rpm; temperature, 25 °C; time, 5 h.
[b] Control experiment conditions: NaOH solution (0.01 M, 0.05 M, 0.07 M,0.1 M, 0.2 M, 0.5 M or 0.7 M), 25 mL; ethanol, 5 mL; benzaldehyde, 1 mL; acetaldehyde, 1 mL; nitrogen atmosphere; temperature, 25 °C; time, 5 h.
[c] The C/O weight ratio has been tested by elemental analysis on a vario EL *III* Elementar.
[d] Carbon balance was measured by equation: $\frac{(\text{GC peak area of product+reactant residual})/(\text{corresponding inert standard peak area})}{(\text{GC peak area of reactant before reaction})/(\text{corresponding inert standard peak area})}$ tetradecane (n-$C_{14}H_{30}$) was used as the inert standard.

Fig. 7. XPS spectra of Pd 3d in Pd/CNS, Pd/CNS-0.1OH, Pd/CNS-0.3OH, Pd/CNS-0.5OH and Pd/CNS-0.7OH catalysts.

−46.4 mV, −47.9 mV, −50.9 mV and −52.3 mV, respectively. The lower zeta potential of alkali-functionalized CNSs with more negatively charged surface is consistently explained by the presence of the above-mentioned two base-induced lactone hydrolysis and carboxyl groups deprotonating reactions, giving rise to the negatively charged –COO– surface functional groups [58,59]. Meanwhile, the lower zeta potential indicates higher surface basicity which may require more protons to neutralize. The pH values of these samples dispersed in distilled water have also been measured for comparison, and results are 6.6, 9.0, 9.2, 9.3, 9.6, 9.8, 10.1 and 10.7 for CNS, CNS-0.1OH, CNS-0.3OH, CNS-0.5OH, CNS-0.7OH, CNS-1OH, CNS-3OH and CNS-5OH, respectively. The surface of pristine CNSs is mildly acidic because of the formation of carboxyl groups during the hydrothermal synthesis of CNSs from glucose. These pH results are in line with the zeta potential measurements, further verifying the increased surface basicity and increased amount of –COO– surface functional groups induced by the increased concentration of sodium hydroxide solution.

To characterize the functionalization of CNSs surfaces using Pd metal NPs, XRD patterns and TEM observations have been carried out. Fig. 5 shows the XRD patterns of Pd-functionalized CNSs catalysts. The diffraction peaks at 40.0° and 46.5° are respectively derived from the (1 1 1) and (2 0 0) planes in the face centered cubic (FCC) crystal structure of Pd [36]. The intensity of Pd characteristic diffraction peaks diminishes with the increase of the alkali solution concentrations. Meanwhile, the increase in the full

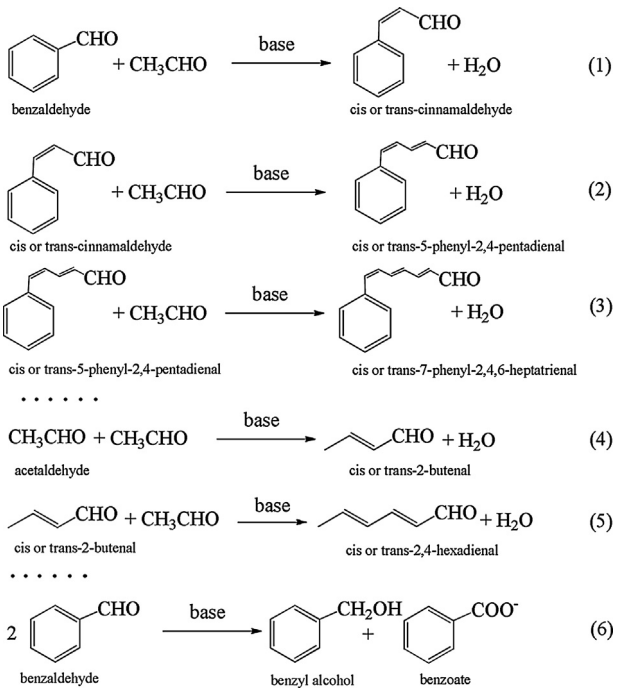

Scheme 3. The main and side reactions during the process of aldol condensation reaction.

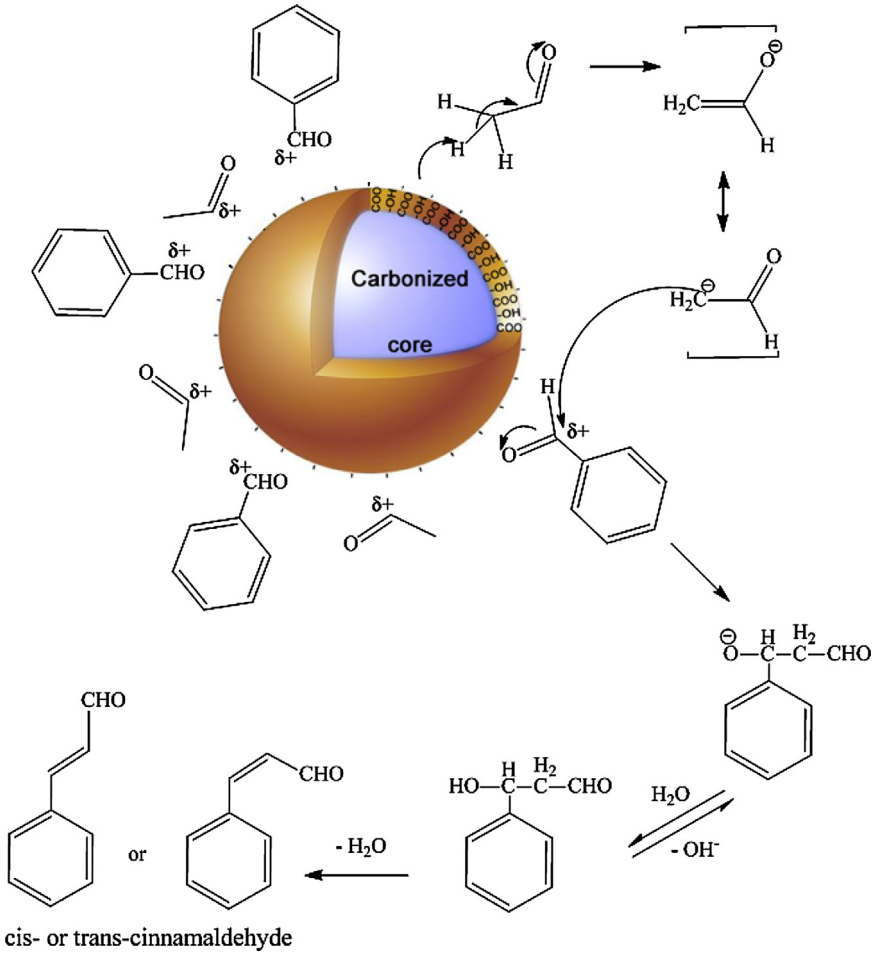

Fig. 8. Schematic diagram of the catalyst-determining mechanism of aldol condensation reaction catalyzed by functionalized CNS activated with alkali aqueous solution.

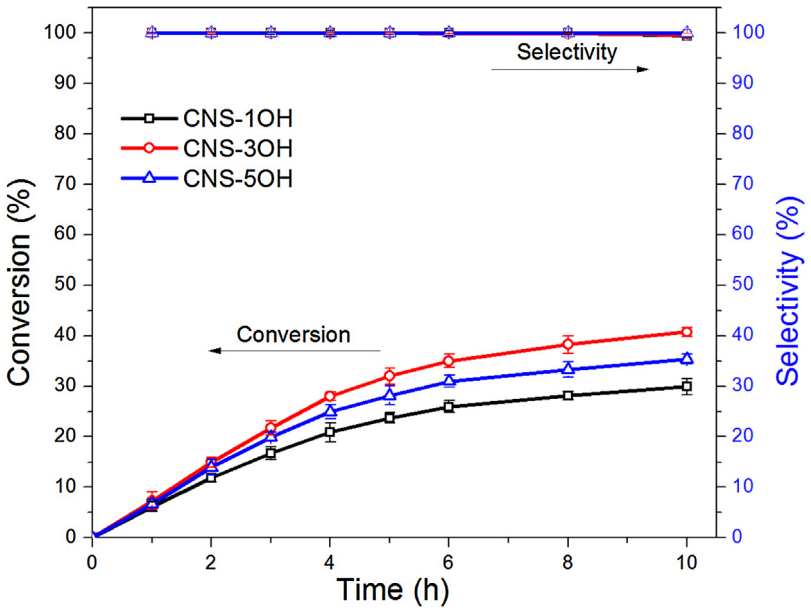

Fig. 9. The conversion-time and selectivity-time curves of aldol condensation reaction to form cinnamaldehyde under reaction condition: functionalized CNS, 0.1 g; H_2O, 10 mL; ethanol, 5 mL; benzaldehyde, 1 mL; acetaldehyde, 1 mL; inert nitrogen atmosphere; stirring rate, 1200 rpm; temperature, 25 °C.

width at half maximum (FWHM) with the decrease of peak intensity indicates the reduced Pd particle size on the CNSs pretreated with higher concentration of NaOH [60,61]. Highly dispersed and small-sized Pd nanoparticles over the surfaces of functionalized CNSs have been further substantiated by TEM observations as displayed in Fig. 6. The average sizes with standard deviations of Pd/CNS, Pd/CNS-0.1OH, Pd/CNS-0.3OH, Pd/CNS-0.5OH and Pd/CNS-0.7OH are 7.5 ± 1.5 nm, 6.1 ± 2.6 nm, 5.1 ± 1.9 nm, 4.2 ± 2.3 nm and 2.7 ± 1.5 nm, respectively. Surface functionalization using alkali solution changes the surface functional groups, decreasing the amounts of lactone or aldehyde groups and increasing the amount of deprotonated carboxylate group which can subsequently increase the surface hydrophilicity and more surface negatively charged sites. The improved hydrophilicity favors the adsorption of Pd^{2+} ions, and the negatively charged surface related to the deprotonated carboxylate group facilitates the electrostatic attraction of the positively charged metallic ions as well as the hydrolysis of Pd^{2+} ions for its immobilization onto the support surfaces. All these factors significantly facilitate the formation of smaller Pd NPs evenly dispersed on the functionalized CNSs support surfaces.

The Pd loadings differ among all these catalysts, illustrated by the ICP results displayed in Table 3. The pristine CNSs without alkali functionalization exhibit the poorest adsorption strength of Pd species. The alkali solution functionalization clearly promotes the metallic ion adsorption on CNSs surfaces. The CNS-0.5OH displays the highest adsorption capacity of Pd species which is in agreement with the study of adsorption kinetics reported by Song et al. [9]. The carbon content detected by elemental analysis for CNS, CNS-0.1OH, CNS-0.3OH, CNS-0.5OH, CNS-0.7OH, CNS-1OH, CNS-3OH and CNS-5OH are 62.1%, 61.9%, 61.5%, 61.3%, 60.8%, 60.1%, 59.6% and 58.9% respectively, with O content of 29.3%, 30.4%, 30.7%, 31.8%, 32.1%, 33.2%, 33.6% and 34.7%, correspondingly. The C/O ratios have been calculated as shown in Tables 1 and 3. With the increase in alkali concentration, there is a minor decrease in C/O weight ratio, with the increase of O atom percentage after the treatment with high concentration of alkali. This is in consistent with the Scheme 2. Alkali solution can catalyze the hydrolysis of lactone and deprotonate the carboxyl group, and can also induce Cannizzaro reaction. Among these reactions, hydrolysis of lactone and Cannizzaro reaction can lead to more O atoms.

The XPS core level spectra of Pd 3d are shown in Fig. 7. The Pd 3d peaks are derived from the Pd $3d_{3/2}$, Pd $3d_{5/2}$ orbitals and each of the two orbitals can be deconvoluted into two peaks because of the presence of two chemical states, the metallic Pd^0 state and cationic Pd^{2+} state [36]. The fractions of Pd^0 (Pd^0/Pd) in Pd/CNS, Pd/CNS-0.1OH, Pd/CNS-0.3OH, Pd/CNS-0.5OH and Pd/CNS-0.7OH are 60.9%, 63.1%, 72.7%, 78.9% and 75.8%, respectively. Surface functionalization by alkali promotes the reduction of Pd. This effect can be strengthened with the increase in alkali concentration until it reaches 0.5 M. During the Pd reduction, suitable surface basicity of functionalized CNSs can reserve the reducibility of the reducing agent $[BH_4]^-$ which would otherwise easily react with the acidic H^+ in the aqueous medium. Nevertheless, highly negatively charged surface may repel the reductive $[BH_4]^-$ anions from approaching the Pd^{2+} adsorbed on the functionalized CNSs surfaces and thus hamper the reduction of Pd^{2+} to form Pd^0. Other explanations include the stronger adsorption of O_2 over the smaller Pd nanoparticles (2.7 nm) may undermine the Pd electron densities on the Pd/CNS-0.7OH catalyst [62]. Moreover, due to the enriched surface functional groups of $-CH_2OH$ and $-COO^-$ generated by the 0.5 M NaOH functionalization, direct redox adsorption of Pd^{2+} ions converting to Pd^0 may also occur on functionalized CNS-0.5OH [9]. Therefore, the Pd/CNS-0.5OH catalyst possesses the highest Pd^0/Pd ratio of 78.9%.

3.2. Catalytic applications of functionalized CNSs

3.2.1. Base-catalyzed selective aldol condensation

Aldol condensation is a well-known base-catalyzed reaction under mild conditions, widely used to achieve the carbon chain growth in aldehyde molecules. The base-functionalized CNSs were employed to serve as the solid base catalyst in aldol condensation between benzaldehyde and acetaldehyde to form cinnamaldehyde. As displayed in Table 1, the NaOH aqueous solution functionalized CNSs is applicable for catalyzing the aldol condensation reaction due to the nature of weak base in the presence of deprotonated $-COO^-$ group and many other oxygen-containing proton acceptors. The NaOH aqueous solutions were also attempted as the catalyst for comparison, showing high conversions but large extent of side reactions as well. The aldol condensation is initiated by the alkali attacking the α-H of aldehyde that is sensitive to strong, steric

Table 2
Effect of temperature on catalytic results of aldol condensation over CNS-3OH.[a]

Entry	Temperature (°C)	Conversion (%)	Yield (%)			Carbon balance of[b]
			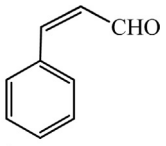 cis- + trans-	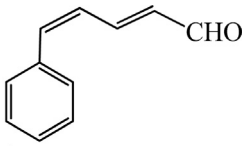 cis- + trans-	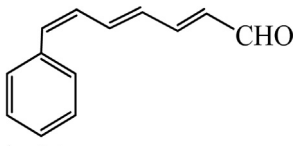 cis- + trans-	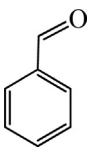
1	20	25.7	25.7	0	0	98.3%
2	25	32.0	32.0	0	0	97.7%
3	30	32.5	32.5	0	0	97.6%
4	35	33.2	32.1	1.1	0	97.3%
5	40	33.9	31.8	2.1	0	97.3%

[a] Reaction conditions: CNS-3OH, 0.1 g; H_2O, 25 mL; ethanol, 5 mL; benzaldehyde, 1 mL; acetaldehyde, 1 mL; nitrogen atmosphere; stirring rate, 1200 rpm; time, 5 h.
[b] Carbon balance was measured by equation: $\frac{(\text{GC peak area of product+reactant residual})/(\text{corresponding inert standard peak area})}{(\text{GC peak area of reactant before reaction})/(\text{corresponding inert standard peak area})}$ tetradecane (n-$C_{14}H_{30}$) was used as the inert standard.

hindrance-free and highly concentrated alkali solutions. NaOH solution with concentration of 0.5 M affords the highest conversion of benzaldehyde while 0.1 M NaOH solution leads to the highest yield toward cinnamaldehyde. Side reactions are inevitable in the strong base catalyzed aldol condensation. The formed cinnamaldehyde further reacts with acetaldehyde in the presence of strong base. In addition, one acetaldehyde molecule can react with another one and the products can further react with acetaldehyde as well. The Cannizzaro reaction may occur in strong basic solutions where the products (i.e., benzyl alcohol and benzoate) can dissolve in the aqueous phase, resulting in the loss of carbon balance. The main and possible side reactions during the aldol condensation process are demonstrated in Scheme 3.

Although the conversions of condensation reactions over CNSs are relatively lower compared to NaOH solutions, the base-functionalized CNSs significantly reduce the types and extents of side reactions. Besides, the carbon balance of benzaldehyde using functionalized CNSs is remarkably better than those using sodium hydroxide. The larger steric hindrance, slower motion and the more moderate basicity make the CNSs solid base attack acetaldehyde at slower rate and therefore averting the rapid emergence of side reactions. Moreover, the negatively charged CNSs surfaces play a role in this highly selective aldol condensation reaction to form cinnamaldehyde according to the mechanism as shown in Fig. 8. The negatively charged CNSs surfaces electrostatically attract the partially positively charged (δ^+) carbonyl carbon. The strength of the partially positive charge (δ^+) on carbonyl carbons of aldehydes decreases in the order as follow because the presence of larger π electron conjugation system can diminish the strength of positive charge on carbonyl group.

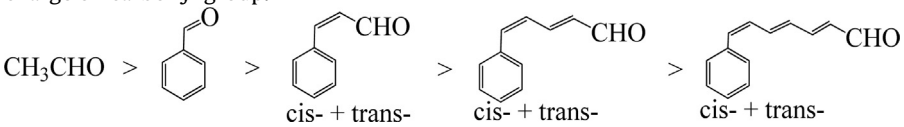

Unless the randomly fast moving acetaldehyde possesses the possibility to provide its α-H for being attacked by the surface basic sites, the carbon anion intermediate instantly attacks the nearby carbonyl groups readily closely located beside the CNSs surface upon the formation of carbon anion intermediate after several electron transferring steps as shown in Fig. 8. The carbon anion intermediate of acetaldehyde can react with either benzaldehyde or acetaldehyde, and the reaction between two acetaldehydes consumes the available acetaldehyde, hampering the objective conversion of benzaldehyde. Since the partially positive charge (δ^+) of the carbonyl group on cinnamaldehyde is even weaker than acetaldehyde or benzaldehyde, the cinnamaldehyde molecules may get far away from the negatively charged CNSs surfaces, the chance of acetaldehyde reacting with cinnamaldehyde is significantly lower, which is the reason why the selectivity toward cinnamaldehyde from benzaldehyde is 100% over CNS-1OH, CNS-3OH and CNS-5OH catalysts without further aldol condensation. Even though the reaction time is prolonged to 10 h, the yields toward cinnamaldehyde are equal or close to the conversion of benzaldehyde, suggesting 100% selectivity as shown by the conversion-time curve combined with the selectivity-time curve plotted in Fig. 9. The CNS-5OH catalyst displays a lower conversion in contrast to CNS-3OH because the stronger surface negative charge possesses the stronger electrostatic attraction toward the partially positively charged (δ^+) carbonyl groups, enhancing the steric hindrance effect and hindering the attack by the carbon anions of acetaldehyde molecules. Therefore, the properly functionalized CNS-3OH presents the highest conversion among all the catalysts and it is selected as the optimal solid base catalyst in aldol condensation reaction for further investigation.

The effect of temperature has been investigated and results are summarized in Table 2. Side reactions are sensitive to temperature because the electrostatic attraction and steric hindrance which determine the selectivity can be undermined by the temperature dependent molecular random motions. High temperature drastically increases the random motion of molecules and subsequently increases the overall conversion at the sacrifice of selectivity or yield toward the desired product. In this study, 30 °C is considered as the optimized reaction temperature for aldol condensation to form cinnamaldehyde over CNS-3OH because of the highest yield and the 100 % selectivity.

Recyclability is investigated in five consecutive runs for the assessment of CNS-3OH catalyst, and the results are shown in Fig. 10. The catalyst is recovered via hot rinsing with ethanol and drying at 40 °C under vacuum. The decrease of conversion, yield and selectivity is insignificant for the first three cycles of reactions, implying the stable catalytic performance of CNS-3OH as a solid base catalyst for aldol condensation. Nonetheless, the diminished conversion, yield and selectivity in the fourth and fifth runs of reaction indicate the loss of basicity and negative charge on the surfaces due to the adsorption of positively charged or acidic molecules. Zeta potential of freshly prepared CNS-3OH is −50.9 mV while the zeta potential of CNS-3OH after 5 consecutive runs of reactions turns out to be −46.2 mV implying the loss of surface negative charge.

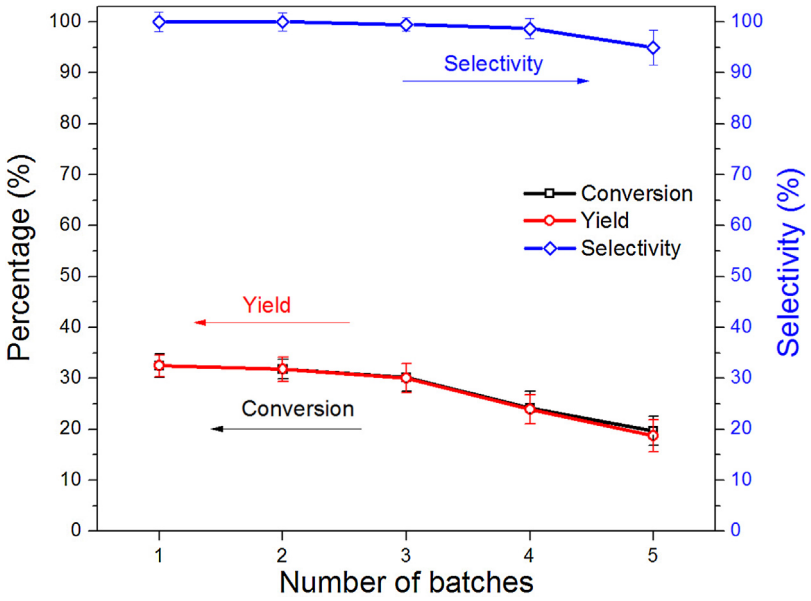

Fig. 10. Recyclability of CNS-3OH catalyst for aldol condensation reaction to form cinnamaldehyde under reaction conditions: CNS-3OH, 0.1 g; H_2O, 10 mL; ethanol, 5 mL; benzaldehyde, 1 mL; acetaldehyde, 1 mL; inert nitrogen atmosphere; stirring rate, 1200 rpm; temperature, 30 °C.

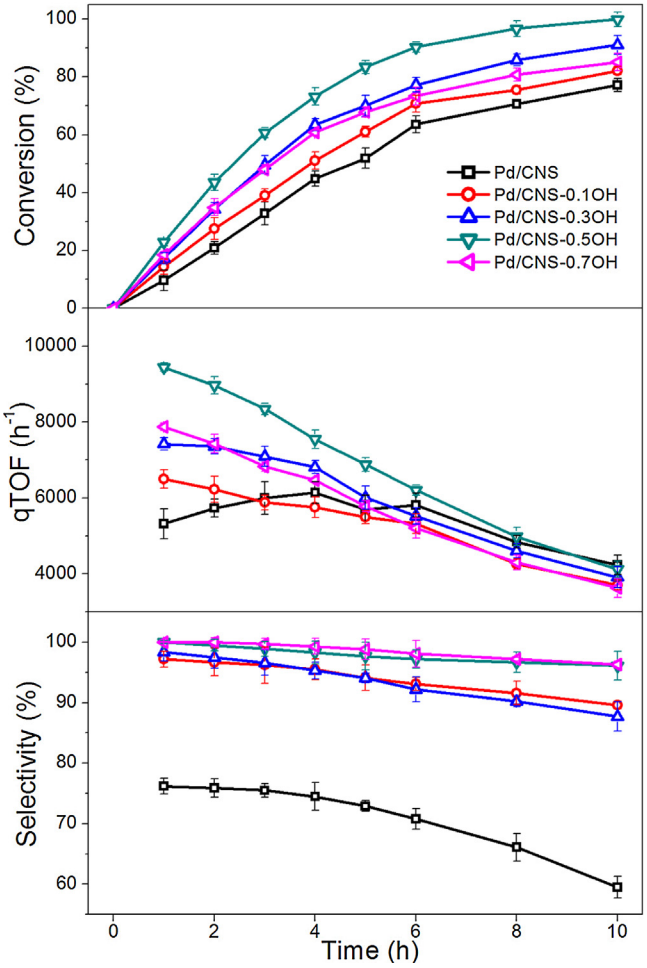

Fig. 11. The conversion, qTOF and selectivity plot as functions of time in benzyl alcohol oxidation reaction. Reaction conditions: catalyst, 10 mg; benzyl alcohol, 50 mmol; temperature, 120 °C; O_2 flow rate, 20 mL min^{-1}; time, 10 h; stirring rate, 1200 rpm.

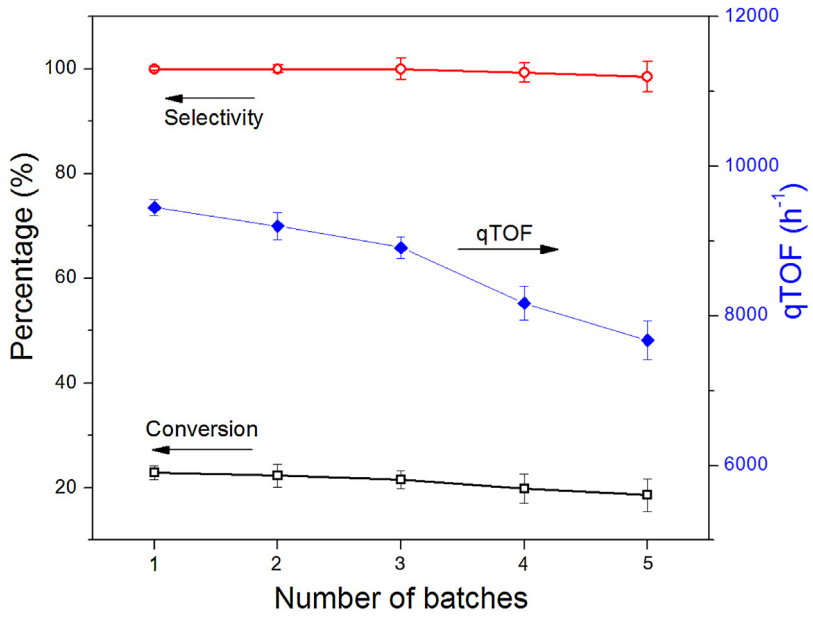

Fig. 12. Recyclability of Pd/CNS-0.5OH catalyst for selective solvent free oxidation of benzyl alcohol under reaction conditions: catalyst, 10 mg; benzyl alcohol, 50 mmol; temperature, 120 °C; O_2 flow rate, 20 mL min^{-1}; time, 1 h; stirring rate, 1200 rpm.

Table 3
Zeta potential, pH and catalytic results of benzyl alcohol oxidation over Pd/CNS, Pd/CNS-0.1OH, Pd/CNS-0.3OH, Pd/CNS-0.5OH and Pd/CNS-0.7OH catalysts.[a]

Entry	Catalyst	ζ Potential of support (mV)	pH of support	Pd[b] (wt.%)	C/O ratio[c]	Conversion (%)	Selectivity (%)			qTOF[d] (h^{-1})	Carbon balance[e]
							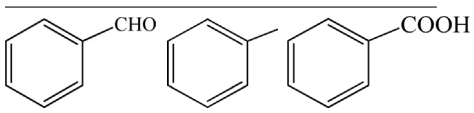				
1	Pd/CNS	−26.8	6.6	1.16	2.12	11.0	76.2	23.5	0.3	5,046	98.8%
2	Pd/CNS-0.1OH	−37.6	9.0	1.18	2.04	14.4	97.2	2.8	0	6,493	98.2%
3	Pd/CNS-0.3OH	−41.8	9.2	1.24	2.00	17.3	98.4	1.6	0	7,424	97.2%
4	Pd/CNS-0.5OH	−43.9	9.3	1.29	1.93	22.9	100	0	0	9,446	97.3%
5	Pd/CNS-0.7OH	−46.4	9.6	1.25	1.89	18.5	100	0	0	7,875	97.9%

[a] Reaction conditions: catalyst, 10 mg; benzyl alcohol, 50mmol; O_2, 20 mL/min; stirring rate, 1200 rpm; temperature, 120 °C; time, 1 h.
[b] Metal content was obtained by ICP.
[c] C/O weight ratio has been tested by elemental analysis on a vario EL *III* Elementar.
[d] qTOF has been derived from the Pd metal content analyzed by ICP.
[e] Carbon balance was measured by equation: $\frac{(\text{GC peak area of product+reactant residual})/(\text{corresponding inert standard peak area})}{(\text{GC peak area of reactant before reaction})/(\text{corresponding inert standard peak area})}$ tetradecane (n-$C_{14}H_{30}$) was used as the inert standard.

3.2.2. *Selective oxidation of benzyl alcohol*

The alkali-functionalized CNSs are further functionalized by Pd nanoparticles and attempted in the solvent-free selective oxidation of benzyl alcohol using gaseous oxygen, and the results are displayed in Table 3. A dramatic increase in the selectivity toward benzaldehyde is observed when functionalizing the CNSs by alkali solutions prior to the decoration of Pd. This result is in agreement with the conclusion drawn by Enache et al. that the acidic nature of catalytic support leads to byproduct formation such as toluene and benzoic acid [63]. The basic and hydrophilic surfaces of catalyst support favor the high dispersion and formation of small sized Pd nanoparticles [36]. According to the TEM observation shown in Fig. 6, the particle size of palladium gradually decreases with the increase of alkali concentration, which is associated with the increased surface basicity and hydrophilicity. However, when the Pd particles are as small as 2.7 nm over CNS-0.7OH, the catalytic activity is not as good as the Pd nanoparticles over CNS-0.5OH. Zhang et al. emphasized the importance of the coordinatively unsaturated sites, such as the edge or corner atoms on the catalytic particle surface for the oxidative dehydrogenation of benzyl alcohol since they are required in the β–H cleavage (i.e., C—H bond activation). Besides, the terrace Pd atoms also play a crucial role in adsorption of benzyl alcohol molecules, which is an important step for its subsequent activation and conversion. Their further computation results exhibit that the Pd nanoparticles sized from 3.6 to 4.3 nm possess the highest TOF for the optimal process of benzyl alcohol adsorption followed by its β-H cleavage [62], which is in agreement with the result that Pd/CNS-0.5OH with the Pd particles sized 4.2 nm possesses the highest catalytic activity.

In addition, the highest electron density of Pd nanoparticles on the Pd/CNS-0.5OH catalyst inspected by XPS may contribute to its catalytic performance for the oxidative dehydrogenation of benzyl alcohol because the high electron density, which is proportional to the Pd^0/Pd fraction, favors the electron transfer and the adsorption of oxygen. Grunwaldt et al. reported that the metallic palladium (Pd^0) was more active catalytic phase for aerobic oxidation of benzyl alcohol than the palladium oxide because the metallic palladium was related to rapid access to adsorbed oxygen [64]. Moreover, Zhu et al. suggested that the surface oxygen-containing species on catalyst support were useful for oxygen activation [65]. Therefore, the Pd/CNS-0.5OH catalyst displays the best catalytic performance by attaining a balance between the electronic effect and the oxygen

Table 4
The catalytic performance of the catalysts below for aerobic oxidation of glycerol.[a]

Entry	Catalyst	Pd[b] (wt.%)	Conversion (%)	Selectivity (%)									qTOF (h^{-1})[c]	Carbon balance[d]
				DHA	GLYA	GLYHD	GLYCA	MOXA	OXA	TARAC	GLYOA	HPYA		
1	Pd/CNS	1.16	13.7	7.5	28.8	1.9	2.6	13.3	33.1	2.4	2.1	8.3	109.3	97.6%
2	Pd/CNS-0.1OH	1.18	17.5	5.6	23.1	1.2	5.4	25.7	30.1	4.4	1.1	3.4	137.2	97.4%
3	Pd/CNS-0.3OH	1.24	21.4	3.9	22.6	0.9	6.2	27.6	29.0	7.0	0.0	2.8	159.7	96.8%
4	Pd/CNS-0.5OH	1.29	20.8	3.2	17.6	0.0	10.0	30.3	28.1	8.6	0.0	2.2	149.2	96.3%
5	Pd/CNS-0.7OH	1.25	18.3	2.3	16.2	0.0	11.4	31.2	26.8	10.1	0.0	2.0	135.5	96.2%

[a] Reaction conditions: 20 mL glycerol aqueous solution (10 wt.%), 50 mg catalyst, O_2 flow rate at 150 mL/min, stirring rate, 1200 rpm; temperature, 80 °C; time, 5 h.
[b] Pd metal contents have been analyzed by ICP.
[c] qTOF = (number of glycerol molecules converted)/(number of Pd atoms)/(reaction time, h).
[d] Carbon balance = the total yield toward DHA, GLYA, GLYHD, GLYCA, MOXA, OXA, TARAC, GLYOA and HPYA. Other byproducts such as CO, CO_2 and HCHO have been detected in gas effluent.

activation. In contrast, the catalytic activity of Pd/CNS-0.7OH is relatively lower due to the small Pd particle size of 2.7 nm, which is inferior to the reactant adsorption over terrace atoms and β–H cleavage over edge or corner atoms. On the other hand, the stronger adsorption of O_2 over Pd particles as small as 2.7 nm and the relatively lower electron density can impede the efficiency of the rapid electron transfer during the oxidation of benzyl alcohol.

The results of carbon balance are slightly smaller than 100% due to the systematic errors and the loss of reactants or products converted into volatile molecules such as CO_2 or CO. The basic surface of catalyst support may also adsorb trace amounts of acidic byproducts.

Fig. 11 exhibits the reaction time dependences of catalytic performances in selective oxidation of benzyl alcohol. All the catalysts possess gradually undermined catalytic performances which are associated with the catalytic activity (qTOF) proportional to decreased slope of the conversion-time curve. The deactivation is resulted from either the coverage of the adsorbed species on Pd surface [66] or the aggregation of Pd particles due to over-oxidation [67]. The hydrocarbon adsorbed on Pd active sites hampers the adsorption of reactants and meanwhile the over-oxidation favors the formation of Pd—O—Pd structure, resulting in larger clusters of particles [43]. Such effects are more apparent for Pd/CNS-0.5OH and Pd/CNS-0.7OH catalysts which demonstrate the faster deactivation. Nonetheless, Pd/CNS demonstrates different catalytic activity trend along with reaction time. It initially shows the lowest conversion and qTOF resulted from the lowest concentration of Pd^0. The increase of catalytic activity during the first four hours can be correlated to the valence transition of Pd upon the adsorption of alcohol molecules which serve as the reducing agent chemically transforming the Pd^{2+} into Pd^0 state [68].

The recyclability of Pd/CNS-0.5OH has been examined and the results for five consecutive reaction cycles are shown in Fig. 12. The catalyst was recovered via hot rinsing with ethanol and drying at 50 °C under vacuum condition and reused in the next batch of reaction. The loss of catalytic activity and selectivity is negligible. The Pd content after the five sequential runs is close to the freshly produced catalyst without obvious leaching due to the strong metal-support interaction after alkali-functionalization of the CNSs surfaces.

3.2.3. Aerobic oxidation of glycerol

Biomass is a renewable resource of fuels and chemicals in bio-refineries where a large amount of inexpensive glycerol has been generated as a by-product [39]. The efficient processes transforming glycerol into valuable chemicals via oxidation in aqueous solutions using gaseous oxygen is an attractive approach [69]. As shown in Table 4, CNSs catalysts functionalized by alkali solutions and Pd nanoparticles have been attempted to catalyze the aerobic oxidation of glycerol to form possible products such as 1,3-dihydroxyaceton (DHA), glyceric acid (GLYA), glyceraldehyde (GLYHD), glycolic acid (GLYCA), mesoxalic acid (MOXA), oxalic acid (OXA), tartronic acid (TARAC), glyoxylic acid (GLYOA) and hydroxypyruvic acid (HYPA), among all of which the high-value products are DHA, GLYA, TARAC and HYPA [38–41].

With the increase in concentration of alkali used to functionalize CNSs, the conversion of glycerol is improved at first and then decreased, with Pd/CNS-0.3OH being the most active catalyst possessing the qTOF of 159.7 h^{-1}. It has been evidenced that basic additive significantly impacts the reaction rate of glycerol oxidation where no catalytic activity was observed in the absence of base addition and the increasing base concentration leads to apparently improved conversion of glycerol [70]. In this study, surface basicity of the CNS catalyst support can enhance the catalytic activity for glycerol conversion in the absence of any basic additives. The catalytic activity increases in the order of Pd/CNS < Pd/CNS-0.1OH < Pd/CNS-0.3OH. Nonetheless, different from the cases where the base is homogeneously dissolved in glycerol aqueous solution, the basic surface of solid catalyst support strongly adsorbs the acidic molecules from abundant acid products and blocks the exposure of metallic active phase. Therefore, the catalytic activity decreases in the order of Pd/CNS-0.3OH > Pd/CNS-0.5OH > Pd/CNS-0.7OH.

The selectivity toward DHA obviously decreases in the order of Pd/CNS > Pd/CNS-0.1OH > Pd/CNS-0.3OH > Pd/CNS-0.5OH > Pd/CNS-0.7OH because DHA is unstable under high pH [70]. In particular, the oxidation of the secondary OH group in glycerol is favored under acidic environment [70–73], nonetheless, strong acidic environment hampers the catalytic activity that glycerol oxidation reaction may stop at a pH as low as 3 [70]. In this study, Pd/CNS possesses the best selectivity toward DHA because of its lowest pH. The glyceraldehyde is unstable and sensitive to basic environment and its selectivity inevitably diminishes when increasing the surface basicity. Since both DHA and glyceraldehyde can interconvert [70], the same trend of selectivity change is reasonable. On the contrary, selectivity toward mesoxalic acid (MOXA) escalates significantly along with either the enhanced surface basicity or the diminished size of Pd nanoparticles, accompanied by the apparently decreased selectivity toward oxalic acid (OXA) which is the most largely produced inexpensive byproduct. In addition, the selectivity toward tartronic acid (TARAC) is improved along with either the enhanced surface basicity or the diminished size of Pd nanoparticles. Accordingly, by controlling both of the surface amphoteric property and diameters of nanoparticles, the selectivity or yield of specifically targeted valuable product can be controlled.

Fig. 13 displays the reaction time dependences of glycerol oxidation over Pd/CNS, Pd/CNS-0.3OH and Pd/CNS-0.7OH catalysts. The conversion gradually increases with decreased reaction rate (i.e., the slope of conversion-time curve) while the selectivities remain constant. The lowest ultimate conversion of glycerol catalyzed by Pd/CNS is attributed to the lowest surface basicity (pH) of cat-

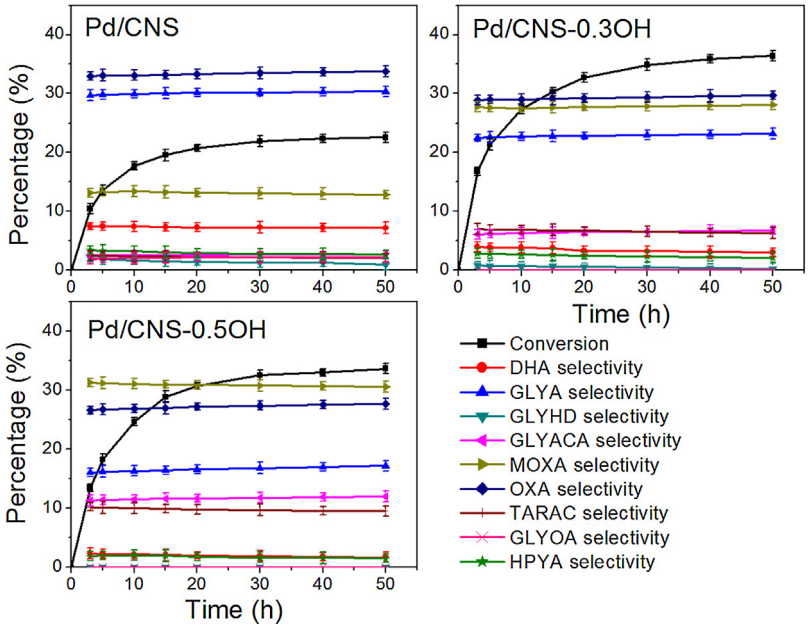

Fig. 13. Time course of the glycerol oxidation over Pd/CNS, Pd/CNS-0.3OH and Pd/CNS-0.7OH catalysts under reaction condition: 20 mL glycerol aqueous solution (10 wt.%), 50 mg catalyst, O_2 flow rate at 150 mL/min, stirring rate, 1200 rpm; temperature, 80 °C.

alyst support [70], which is in agreement with previous results. Drastically diminished slope of the conversion-time curve in glycerol oxidation catalyzed by Pd/CNS-0.7OH implies the apparent decrease of reaction rate due to the catalytic deactivation because the Pd nanoparticles as small as 2.7 nm on Pd/CNS-0.7OH can be easily blocked by the strongly adsorbed acidic species. On the other hand, the steady selectivity values infer that the influence of catalyst properties on selectivity distributions may surpass the effect of reaction time and this is in agreement with the results reported by Hirasawa et al. [69]. Pd/CNS-0.3OH possesses the highest ultimate conversion of glycerol and the decrease in slope of conversion-time curve is not as rapid as either Pd/CNS or Pd/CNS-0.7OH, implying the relatively enhanced anti-deactivation capability.

4. Conclusions

CNSs have been hydrothermally synthesized and post-functionalized by alkali aqueous solutions. The afforded solid base catalysts showed remarkably high selectivity toward targeted aldehyde in aldol condensation with reasonable catalytic activity. Among all the tested catalysts, CNSs with moderate amounts of surface functional groups displayed the optimal conversion, selectivity and yield toward cinnamaldehyde due to its large steric hindrance, slow motion compared to OH^- ions, appropriate basicity and the negatively charged surface which are vital factors for the catalyst-determining reaction mechanism. The alkali-functionalized CNSs were further functionalized by decorating Pd nanoparticles and the as-synthesized catalysts were employed in the selective oxidation of benzyl alcohol and the aerobic oxidation of glycerol. Surface basicity, electron density and diameters of Pd nanoparticle were critical in these catalytic reactions.

Acknowledgement

This project is funded by the National Research Foundation (NRF), Prime Minister's Office, Singapore under its Campus for Research Excellence and Technological Enterprise (CREATE) program. Authors also thank to the financial support from AcRF Tier 1 grant (RG129/14), Ministry of Education, Singapore.

References

[1] Y. Yan, J. Miao, Z. Yang, F.-X. Xiao, H.B. Yang, B. Liu, Y. Yang, Chem. Soc. Rev. 44 (2015) 3295–3346.
[2] D.S. Yuan, C.W. Xu, Y.L. Liu, S.Z. Tan, X. Wang, Z.D. Wei, P.K. Shen, Electrochem. Commun. 9 (2007) 2473–2478.
[3] E. Hammel, X. Tang, M. Trampert, T. Schmitt, K. Mauthner, A. Eder, P. Potschke, Carbon 42 (2004) 1153–1158.
[4] A. Hashimoto, K. Suenaga, A. Gloter, K. Urita, S. Iijima, Nature 430 (2004) 870–873.
[5] D.S. Yu, K. Goh, H. Wang, L. Wei, W.C. Jiang, Q. Zhang, L.M. Dai, Y. Chen, Nat. Nanotechnol. 9 (2014) 555–562.
[6] C.W. Xu, Y.L. Liu, D.S. Yuan, Int. J. Electrochem. Sci. 2 (2007) 674–680.
[7] E. Auer, A. Freund, J. Pietsch, T. Tacke, Appl. Catal. Gen. 173 (1998) 259–271.
[8] C.W. Xu, L.Q. Cheng, P.K. Shen, Y.L. Liu, Electrochem. Commun. 9 (2007) 997–1001.
[9] X.H. Song, P. Gunawan, R.R. Jiang, S.S.J. Leong, K.A. Wang, R. Xu, J. Hazard. Mater. 194 (2011) 162–168.
[10] V. Vignal, A.W. Morawski, H. Konno, M. Inagaki, J. Mater. Res. 14 (1999) 1102–1112.
[11] M. Inagaki, V. Vignal, H. Konno, A.W. Morawski, J. Mater. Res. 14 (1999) 3152–3157.
[12] Y.N. Xia, B. Gates, Y.D. Yin, Y. Lu, Adv. Mater. 12 (2000) 693–713.
[13] S. Flandrois, B. Simon, Carbon 37 (1999) 165–180.
[14] Z.H. Yi, Y.G. Liang, X.F. Lei, C.W. Wang, J.T. Sun, Mater. Lett. 61 (2007) 4199–4203.
[15] J. Hu, H. Li, X.J. Huang, Solid State Ionics 178 (2007) 265–271.
[16] X.M. Sun, Y.D. Li, Angew. Chem. Int. Ed. 43 (2004) 3827–3831.
[17] R.Z. Yang, H. Li, X.P. Qiu, L.Q. Chen, Chem. Eur. J. 12 (2006) 4083–4090.
[18] X.L. Li, T.J. Lou, X.M. Sun, Y.D. Li, Inorg. Chem. 43 (2004) 5442–5449.
[19] P. Serp, R. Feurer, P. Kalck, Y. Kihn, J.L. Faria, J.L. Figueiredo, Carbon 39 (2001) 621–626.
[20] M. Washiyama, M. Sakai, M. Inagaki, Carbon 26 (1988) 303–307.
[21] Z.L. Wang, Z.C. Kang, J. Phys. Chem. 100 (1996) 17725–17731.
[22] Z.S. Lou, Q.W. Chen, J. Gao, Y.F. Zhang, Carbon 42 (2004) 229–232.
[23] X.M. Sun, Y.D. Li, J. Colloid Interface Sci. 291 (2005) 7–12.
[24] X.M. Sun, Y.D. Li, Angew. Chem. Int. Ed. 43 (2004) 597–601.
[25] Y. Wan, Y.L. Min, S.H. Yu, Langmuir 24 (2008) 5024–5028.
[26] M.T. Zheng, Y.L. Liu, Y. Xiao, Y. Zhu, Q. Guan, D.S. Yuan, J.X. Zhang, J. Phys. Chem. C 113 (2009) 8455–8459.
[27] Y. Shin, L.Q. Wang, I.T. Bae, B.W. Arey, G.J. Exarhos, J. Phys. Chem. C 112 (2008) 14236–14240.
[28] M. Li, W. Li, S. Liu, Carbohydr. Res. 346 (2011) 999–1004.
[29] R. Demir-Cakan, N. Baccile, M. Antonietti, M.M. Titirici, Chem. Mater. 21 (2009) 484–490.
[30] Y.H. Ni, L.N. Jin, L. Zhang, J.M. Hong, J. Mater. Chem. 20 (2010) 6430–6436.
[31] L.F. Lai, G.M. Huang, X.F. Wang, J. Weng, Carbon 48 (2010) 3145–3156.
[32] X.M. Sun, J.F. Liu, Y.D. Li, Chem. Eur. J. 12 (2006) 2039–2047.
[33] H.S. Qian, G.F. Lin, Y.X. Zhang, P. Gunawan, R. Xu, Nanotechnology 18 (2007).
[34] Y.J. Jiang, X.T. Li, Q.A. Cao, X.D. Mu, J. Nanopart. Res. 13 (2011) 463–469.
[35] G.D. Yadav, G.P. Fernandes, Catal. Today 207 (2013) 162–169.

[36] Y.B. Yan, Y.T. Chen, X.L. Jia, Y.H. Yang, Appl. Catal. B Environ. 156 (2014) 385–397.
[37] A. Savara, C.E. Chan-Thaw, I. Rossetti, A. Villa, L. Prati, Chemcatchem 6 (2014) 3464–3473.
[38] R.F. Nie, D. Liang, L. Shen, J. Gao, P. Chen, Z.Y. Hou, Appl. Catal. B Environ. 127 (2012) 212–220.
[39] J.J. Bozell, G.R. Petersen, Green Chem. 12 (2010) 539–554.
[40] M. Pagliaro, R. Ciriminna, H. Kimura, M. Rossi, C. Della Pina, Angew. Chem. Int. Ed. 46 (2007) 4434–4440.
[41] B. Katryniok, H. Kimura, E. Skrzynska, J.S. Girardon, P. Fongarland, M. Capron, R. Ducoulombier, N. Mimura, S. Paul, F. Dumeignil, Green Chem. 13 (2011) 1960–1979.
[42] H. Sun, Q.H. Tang, Y. Du, X.B. Liu, Y. Chen, Y.H. Yang, J. Colloid Interface Sci. 333 (2009) 317–323.
[43] H.T. Tan, Y.T. Chen, C.M. Zhou, X.L. Jia, J.X. Zhu, J. Chen, X.H. Rui, Q.Y. Yan, Y.H. Yang, Appl. Catal. B Environ. 119 (2012) 166–174.
[44] A.J. Romero-Anaya, M. Ouzzine, M.A. Lillo-Ródenas, A. Linares-Solano, Carbon 68 (2014) 296–307.
[45] X.B. Wu, P. Chen, J. Lin, K.L. Tan, Int. J. Hydrogen Energy 25 (2000) 261–265.
[46] E.N. Konyushenko, J. Stejskal, M. Trchova, J. Hradil, J. Kovarova, J. Prokes, M. Cieslar, J.Y. Hwang, K.H. Chen, I. Sapurina, Polymer 47 (2006) 5715–5723.
[47] Y.K. Kim, H. Park, Energy Environ. Sci. 4 (2011) 685–694.
[48] P.E. Fanning, M.A. Vannice, Carbon 31 (1993) 721–730.
[49] C. Lievens, D. Mourant, M. He, R. Gunawan, X. Li, C.-Z. Li, Fuel 90 (2011) 3417–3423.
[50] I. Novak, P. Sysel, J. Zemek, M. Spirkova, D. Velic, M. Aranyosiova, S. Florian, V. Pollak, A. Kleinova, F. Lednicky, I. Janigova, Eur. Polym. J. 45 (2009) 57–69.
[51] X.G. Sun, Spectrochim. Acta Part Mol. Biomol. Spectrosc. 62 (2005) 557–564.
[52] C. Yao, Y. Shin, L.Q. Wang, C.F. Windisch, W.D. Samuels, B.W. Arey, C. Wang, W.M. Risen, G.J. Exarhos, J. Phys. Chem. C 111 (2007) 15141–15145.
[53] S. Shin, J. Jang, S.H. Yoon, I. Mochida, Carbon 35 (1997) 1739–1743.
[54] A. Afkhami, T. Madrakian, Z. Karimi, A. Amini, Colloids Surf. Physicochem. Eng. Aspects 304 (2007) 36–40.
[55] J.P. Chen, S.N. Wu, Langmuir 20 (2004) 2233–2242.
[56] P. Pendleton, S.H. Wu, A. Badalyan, J. Colloid Interface Sci. 246 (2002) 235–240.
[57] A. Weissberger, R. Haase, Journal of the Chemical Society (1934) 535-536.
[58] S.F. Wu, K. Yanagisawa, T. Nishizawa, Carbon 39 (2001) 1537–1541.
[59] H. Sis, M. Birinci, Colloids Surf. Physicochem. Eng. Aspects 341 (2009) 60–67.
[60] H.G. Jiang, M. Ruhle, E.J. Lavernia, J. Mater. Res. 14 (1999) 549–559.
[61] A.L. Patterson, Phys. Rev. 56 (1939) 978–982.
[62] Q.H. Zhang, W.P. Deng, Y. Wang, Chem. Commun. 47 (2011) 9275–9292.
[63] D.I. Enache, J.K. Edwards, P. Landon, B. Solsona-Espriu, A.F. Carley, A.A. Herzing, M. Watanabe, C.J. Kiely, D.W. Knight, G.J. Hutchings, Science 311 (2006) 362–365.
[64] J.-D. Grunwaldt, M. Caravati, A. Baiker, J. Phys. Chem. B 110 (2006) 25586–25589.
[65] J. Zhu, S.A.C. Carabineiro, D. Shan, J.L. Faria, Y. Zhu, J.L. Figueiredo, J. Catal. 274 (2010) 207–214.
[66] T. Suzuki, R. Souda, Surf. Sci. 448 (2000) 33–39.
[67] P. Maity, C.S. Gopinath, S. Bhaduri, G.K. Lahiri, Green Chem. 11 (2009) 554–561.
[68] F. Li, Q.H. Zhang, Y. Wang, Appl. Catal. Gen. 334 (2008) 217–226.
[69] S. Hirasawa, H. Watanabe, T. Kizuka, Y. Nakagawa, K. Tomishige, J. Catal. 300 (2013) 205–216.
[70] E.G. Rodrigues, S.A.C. Carabineiro, J.J. Delgado, X. Chen, M.F.R. Pereira, J.J.M. Orfao, J. Catal. 285 (2012) 83–91.
[71] B.N. Zope, D.D. Hibbitts, M. Neurock, R.J. Davis, Science 330 (2010) 74–78.
[72] G.J. Hutchings, S. Carrettin, P. Landon, J.K. Edwards, D. Enache, D.W. Knight, Y.J. Xu, A.F. Carley, Topics Catal. 38 (2006) 223–230.
[73] S. Demirel-Gulen, M. Lucas, P. Claus, Catal. Today 102 (2005) 166–172.